Journal of Neuroscience Research

WILEY

JOURNAL OF Neuroscience Research

RESEARCH ARTICLE OPEN ACCESS

Effect of Anesthesia and Diurnal Variation on Chronic Vagus Nerve Activity in Rats

Aaron J. Rodrigues | Joseph T. Marmerstein | Bhanu P. Kotamraju | Grant A. McCallum | Dominique M. Durand

Neural Engineering Center, Department of Biomedical Engineering, Case Western Reserve University, Cleveland, Ohio, USA

Correspondence: Dominique M. Durand (dxd6@case.edu)

Received: 5 September 2024 | **Revised:** 12 April 2025 | **Accepted:** 1 May 2025

Editor: Edited by Lawrence S. Sherman and Lindsay R Halladay. Reviewed by James Henry Peters, Riëm El Tahry and David Kline

Funding: This work was supported by National Institutes of Health (Nerve reshaping for improved selectivity, 5R01NS032845-22).

Keywords: autonomic nervous system | carbon nanotube yarn electrodes | circadian rhythms | diurnal variation | isoflurane anesthesia | sample entropy | vagus nerve

ABSTRACT

The vagus nerve, serving as a pivotal link between the brain and vital organs, regulates crucial physiological functions. It plays a central role in maintaining homeostasis within the body and must dynamically adapt to changing conditions such as anesthesia or sleep. While vagal tone, typically estimated indirectly from heart rate variability, has been extensively studied, direct measurement of vagal activity during sleep and anesthesia remains unreported to date. Recent technological advancements have facilitated the recording of vagus nerve activity in freely moving rodents using small, highly flexible carbon nanotube yarns. Consequently, it is now feasible to directly investigate vagal activity during events known to impact homeostasis, such as diurnal variations and anesthesia. In this study, we explore the relationship between anesthesia and vagus nerve activity by comparing the effects of 2% isoflurane anesthesia with activity in freely moving male Sprague Dawley rats. The findings reveal that 2% isoflurane anesthesia significantly suppresses vagus nerve activity, and normal activity levels do not resume until 2 h after the termination of the anesthesia supply. Additionally, we examine the influence of diurnal variations on vagus nerve activity and observe a notable presence of diurnal variations in vagal activity patterns. These results provide insights into the interaction among anesthesia, diurnal variations, and vagal tone, offering valuable understanding of the autonomic nervous system during critical physiological states.

1 | Introduction

The vagus nerve is a paramount conduit between the brain and several vital organs, as it plays a crucial role in regulating heart rate, digestion, breathing, and stress response (Berthoud and Neuhuber 2000; Breit et al. 2018; Browning et al. 2017; Wagner 2022). The use of vagus nerve stimulation (VNS) for treating epilepsy, obesity, and depression has increased interest in the nerve's underlying physiological mechanisms (Cracchiolo et al. 2021; Groves and Brown 2005; Johnson and Wilson 2018; Pardo et al. 2007). Although vagus nerve stimulation is now standard of care, vagus nerve recording has proved more difficult to achieve. Yet, direct measurement of vagus nerve activity would be crucial for decoding efferent and afferent signals coming from and going to organs in the body. In particular, the ability to understand vagal signals during periods of physiological changes, such as diurnal variations and anesthesia, could be crucial for understanding the underlying mechanisms of homeostasis.

To implement chronic neural recordings in freely moving animals with high selectivity and signal-to-noise ratio (SNR), we

Summary

- This study shows that anesthesia significantly reduces brain input by suppressing vagus nerve activity.
- Since 80% of vagal fibers transmit information from the body to the brain, this suppression means the brain receives much less sensory input during anesthesia.
- To record from freely moving subjects, we employed advanced chronic recording techniques and introduced sample entropy as a novel measure of neural complexity.
- The study also finds a strong correlation between vagus nerve activity and diurnal variations, suggesting that timing could be crucial for optimizing treatments for diseases related to the autonomic nervous system, including obesity, depression, and cardiovascular disorders.

used an intrafascicular carbon nanotube yarn (CNTY) interface. CNTYs are highly flexible, small in diameter (10–20 μm), and were placed within the perineurium to keep electrode contacts in close proximity to nerve fibers (McCallum et al. 2017). Compared to the widely used cuff electrodes, which detect small local field potentials outside the electrically insulating perineurium layer, CNTYs can provide low impedance, high entropy, high signal-to-noise ratios, and high longevity (Kotamraju et al. 2023; Wodlinger and Durand 2009). By using CNTYs and developing techniques to record nerve activity in non-anesthetized rats, the first direct measurements of vagal tone in freely moving animals have been recorded successfully (Marmerstein et al. 2021). This study uses CNTYs to record over 750 h of electroneurogram (ENG) data from 7 subjects, which enables comprehensive analysis on the effect of isoflurane anesthesia and diurnal variations on chronic vagus nerve activity.

Several studies have provided insights into the impact of anesthesia on the vagus nerve under various conditions. Silverman et al. (2018) used hook and cuff electrodes to record baseline vagus nerve activity at different isoflurane levels (1.5%, 1.75%, and 2.0%) and reported that higher anesthesia levels significantly inhibited vagus nerve activity. Other studies have measured the effect of anesthesia on vagal tone via indirect means, the most common being heart rate variability (HRV). It has been hypothesized that increased heart rate during anesthesia administration is caused by inhibited vagal activity (Bouairi et al. 2004; Chapleau and Sabharwal 2011; Halliwill and Billman 1992; Picker et al. 2001). The impact of anesthesia on VNS is also a subject of significant interest. Ahmed et al. (2021) found that anesthesia, particularly isoflurane, significantly influences the stimulation dose calibration for VNS in both acute and chronic implants. Picq et al. (2013) found that the choice of anesthetic agents, between isoflurane and pentobarbital, significantly affects the immune response and cellular dynamics in a VNS rat model. Although chronic, freely moving rodent studies have observed reduced vagal activity under anesthetized conditions (Falcone et al. 2020; Marmerstein et al. 2021), there has been little direct examination of vagus nerve activity during the transition from anesthesia to wakefulness. Falcone et al. (2020) specifically reported chronic, awake vagus nerve recordings in mice, noting a reduction in neural signal during anesthesia recovery. While these studies observe reduced activity during the recovery period, they do not fully characterize the duration or temporal patterns of vagal recovery post-anesthesia. This study not only examines the suppression of vagus nerve activity during anesthesia, but also characterizes the duration and dynamics of vagal recovery from anesthesia in rats.

The vagus nerve is deeply involved in diurnal variations, influencing temporal patterns across various physiological systems. Bando et al. (2007) demonstrated that rhythmic signals from the central circadian clock are transmitted via the vagus nerve to peripheral tissues, influencing respiratory functions. Similarly, Black et al. (2019) highlighted circadian rhythms in cardiac electrophysiology, regulated by central and local clock mechanisms and involving vagal pathways. Woodie et al. (2024) demonstrated that hepatic vagal afferents transmit clock-dependent signals, highlighting the vagus nerve's role in systemic circadian regulation. Smets et al. (2022) directly recorded vagus nerve activity, observing cyclical patterns over the light–dark cycle, further supporting the link between vagal activity and diurnal variations. These studies suggest that vagal signaling is integral to diurnal regulation, yet much of the existing evidence derives from indirect measures such as HRV (Burgess et al. 1997; Li et al. 2011; Oosting et al. 1997). Building on this foundation, this study explores how diurnal rhythms intersect with the dynamics of vagal activity during recovery from anesthesia, a topic that remains largely unexplored. By recording direct vagus nerve activity during the transition from anesthesia to wakefulness, we provide evidence that while anesthesia significantly suppresses vagal tone, anesthesia recovery aligns with the expected diurnal patterns of vagus nerve activity. These findings demonstrate that diurnal variations are preserved during recovery, offering novel insights into temporal regulation during anesthesia recovery and informing potential time-based interventions targeting vagal modulation.

To characterize vagus nerve activity, previous studies have used root-mean-square (RMS) and spike-rate (Marmerstein et al. 2022, 2021; McCallum et al. 2020, 2017; Smets et al. 2022), since RMS provides an estimate of the overall power of nerve signals and spike-rate quantifies the firing patterns within the vagus nerve. In this study, we also introduce the use of sample entropy for quantifying the complexity of vagus nerve spike trains. Previous studies have effectively applied sample entropy for HRV analysis to capture variations in the time series of successive heartbeats (Lake et al. 2002; Richman and Moorman 2000; Yan et al. 2022). Unlike Shannon entropy, which has been recently explored for measuring information content in sciatic nerve spike trains (Kotamraju et al. 2023), sample entropy specifically captures temporal complexity and recurrence patterns in spike trains, providing a more comprehensive understanding of the neural dynamics at play (Delgado-Bonal and Marshak 2019; Nagaraj and Balasubramanian 2017; Richman and Moorman 2000; Strong et al. 1998).

In this study, we compare recordings of vagus nerve activity between anesthetized and non-anesthetized subjects using a chronic preparation. We show the residual effects of anesthesia by monitoring vagus nerve activity after terminating anesthesia supply. We also report the significant presence of diurnal

variations in vagus nerve activity. We report that anesthesia with 2% isoflurane significantly suppresses vagus nerve activity, with suppression continuing for an additional 2 h after terminating anesthesia administration.

2 | Materials and Methods

CNTY electrode manufacture, surgical, and recording procedures are similar to those previously published (Marmerstein et al. 2022; McCallum et al. 2017). They are briefly described here, as are the signal processing and statistical methods used.

2.1 | Electrode Manufacture

CNTY electrodes consist of two parts: a CNT yarn that interfaces with the nerve and a DFT end that connects to the percutaneous port. CNT yarn (manufactured at Case Western Reserve University as described in Qu et al. 2008) was attached to 35NLT-DFT wire (Fort Wayne Metals, Fort Wayne, IN, USA) with silver conductive epoxy (H20E, EPO-TEK). The junction was sealed with Dacron mesh and silicone elastomer (MED-4211/MED-4011, NuSil Silicone Technology, Carpinteria, CA, USA). A fisherman's knot was used to tie the free end of the CNTY to the end of an 11-0 nylon suture. Parylene-C (5 μm thick vapor deposition coating, SMART Microsystems, Elyria, OH, USA) was used to coat the entire CNTY. Then, a laser spot welder (KelanC Laser, set to 1A current, 0.3 ms pulse width, and 300 μm spot diameter) was used to remove around 200 μm of parylene-C approximately 500 μm behind the CNTY-suture knot (see Marmerstein et al. 2022; McCallum et al. 2017 for additional details).

2.2 | Surgery

All surgical and experimental procedures were carried out with the approval and oversight of the Case Western Reserve University Institutional Animal Care and Use Committee to ensure compliance with all federal, state, and local animal welfare laws and regulations (protocol 2016–0328). Electrodes were implanted in seven male Sprague Dawley rats between 7 and 12 weeks of age. To implant the CNTY electrodes, the suture was sewn through the left cervical vagus nerve for ~2 mm and pulled until the CNTY-suture knot emerged just outside the nerve. To ensure that the recording site remained inside the nerve, the electrode was pulled back until the knot sat against the perineurium, and the nerve, electrodes, and junctions were covered with ~1 mL of fibrin glue (Tisseel, Baxter International Inc., Deerfield, IL, USA). Two electrodes were implanted with ~2 mm separation inside the vagus nerve (ENG), and two electrodes were placed with ~2 mm separation extraneurally near the vagus implant site. The extraneural electrodes served as a control during recording sessions to detect common-mode signals and reject high-noise time periods. The DFT wires were tunneled from the neck to the back of the skull and soldered to a 5-pin Omnetics connector (Omnetics Connector Corporation MCP-5-SS) fixed on top of the skull with dental cement. The amplifier ground was connected to a screw placed in the skull. Animals were anesthetized using 2% isoflurane delivered in 1 L/min oxygen during surgery. Postoperative analgesia included 5 mg/kg Carprofen subcutaneously before surgery and every 24 h for 2–3 days, and 1 mL of lidocaine injected subcutaneously at the incision site prior to surgery. All subjects were monitored for 5 days postoperatively and provided with 5 mL warmed lactated Ringer's solution subcutaneously for hydration. They were placed on heating pads during and after surgery and offered easily accessible food, including softened chow and DietGel 76A (ClearH2O, Westbrook, ME, USA). A one-week recovery period was observed after which neural recordings were obtained. During non-anesthetized recordings, subjects were given unrestricted access to standard rodent food and water, and were kept in regular cages under a typical 12-h light/dark cycle. (see Marmerstein et al. 2022 for additional details).

2.3 | Neural Recording

For each of the 7 male Sprague Dawley rats, a custom-built PCB with an Intan RHD2216 recording chip was attached to the headcap connector, which was secured to the animal with a 3D-printed locking mechanism and attached to a PlasticsOne (Roanoke, VA, USA) commutator to allow free movement of the animals in the cage. Input signals from the two bipolar electrodes (ENG and extraneural) were routed to amplifier channels, with 6 parallel channels used per electrode. Output from the amplifier board was run through the commutator into an Intan RHD USB Interface board (Intan part #C3100) that was powered by an external battery supplying 5 V DC power. Recorded signals were filtered with a 5 kHz low-pass filter and sampled at 20 kHz. To manage multi-channel high-frequency data, continuous recordings were saved in 10-min intervals as individual files. During ENG recording, a video camera equipped with an infrared light and infrared sensor was used for simultaneous video recording (see Marmerstein et al. 2022 for additional details).

Of the total of 7 animals, recordings from 5 animals contributed to the anesthetized group and recordings from 4 animals to the non-anesthetized group. Two subjects were common in both groups, with recordings for each condition performed on separate days. To ensure no carryover effects from anesthesia, a minimum recovery period of 8 h post-anesthesia was required before subjects were considered non-anesthetized for Sections 3.1, 3.2, and 3.4. For example, if a subject was removed from anesthesia at 3 pm, only data from the following days (12 am after) were used for the non-anesthetized condition. Data collected between the anesthetized and non-anesthetized conditions were used for the anesthesia recovery analysis (see Section 3.3). Only data from the non-anesthetized condition were used in the diurnal variations analysis (see Section 3.4). 772.3 h of ENG data were recorded across all subjects; see Table S1 for details. Data associated with this study are available through the SPARC Portal (RRID: SCR_017041) under a CC-BY-4.0 license (Marmerstein et al. 2023).

2.4 | Signal Processing

ENG and extraneural (control) data were imported into MATLAB (version R2021b, Mathworks) for processing. The

six parallel amplifier channels of differential recording data from each electrode were averaged with software to decrease amplifier noise (Dweiri et al. 2015). The data were digitally filtered from 500 to 1200 Hz with a 7th order, zero-phase, Butterworth bandpass filter to minimize interference from EMG, ECG, and other noise sources (e.g., white noise, triboelectric noise, electromagnetic noise; Diedrich et al. 2003; Kotamraju et al. 2023; McCallum et al. 2020). Recording intervals were excluded if the normalized cross-correlation between intraneural and extraneural data exceeded 0.3, as high correlations indicated noise leakage into the ENG recording. The cross-correlation was computed over a 2-s window, and the threshold was based on Cohen's guidelines for moderate correlation strength to ensure reliable identification of compromised intervals (Cohen 1988). Wavelet symlets 7 (sym7) were employed for wavelet denoising (Diedrich et al. 2003; Micera et al. 2011). Wavelet decomposition was performed over 4 levels, and hard thresholding was applied to each level's coefficients based on their standard deviations. The full set of decomposed levels was used for signal reconstruction. For each subject and day, the baseline ENG RMS (root mean squared) value was determined as the lowest RMS found within a 10 ms window across the entire day. To calculate the peak-to-peak ENG threshold, this daily baseline was multiplied by 4.5, resulting in thresholds typically around 10 μV across subjects. Thresholds ranging from 3 times to 8 times RMS have been reported in prior studies (Jiman et al. 2020; Kotamraju et al. 2023; Marmerstein et al. 2022; McCallum et al. 2020). While this multiplier is less conservative than the 6–8 times RMS thresholds used in previous analyses of this data (Marmerstein et al. 2022, 2021), our preliminary analyses showed it more reliably balanced detection sensitivity while maintaining specificity. This threshold identification method was repeated with extraneural data to determine the baseline extraneural RMS and peak-to-peak extraneural threshold for each day and subject. When extraneural data samples exceeded the extraneural threshold, concurrent ENG data samples were removed to reduce false positive signals. See Figure S1 for an example of common activity filtering using extraneural data. Following this procedure, any recording intervals with less than 2 min of ENG data remaining (i.e., 20% of the original recording interval) were excluded (this most commonly occurred in non-anesthetized recordings). See Table S2 for a comparison between the initial data volume and the amount remaining after filtering and denoising. Positive thresholding was applied to identify spike amplitudes in ENG data using the ENG threshold. Because multiple neurons within the vagus nerve fascicle can produce overlapping action potentials near the site of electrode implantation, no minimum peak distance was used to filter spike detection, allowing for the accurate detection of closely spaced spikes from different axons. The number of spikes was counted as shown in Figure 5c, where 13 peaks in a 100 ms window for a non-anesthetized subject correspond to 130 spikes/s. If spike sorting were performed on this data to filter out overlapping action potentials, the average spike rate was around 10 spikes/s (see Marmerstein et al. 2022 for additional details); this aligns with existing literature in which spike sorting was performed on vagus nerve spike trains (Jiman et al. 2020; McCallum et al. 2017). To calculate sample entropy, spike counts were divided into non-overlapping 50 ms bins and categorized into spike count ranges (e.g., 0–5, 6–10, 11–15 spikes), with a cap at 50 spikes per bin to reduce the effect of skewed distributions. This categorized vector was then used in the formula shown in Equation (1).

$$\text{SampEn} = -\ln\left(\frac{A}{B} \times \frac{N-m+1}{N-m-1}\right) \tag{1}$$

With $m=2, r=0.2$, where A is the number of $m+1$-dimensional vectors within distance r of each other, B is the number of m-dimensional vectors within distance r of each other, r is the tolerance threshold, and N is the number of timepoints (Richman and Moorman 2000). The parameter $m=2$ was chosen based on typical recommendations for physiological data, with values between 2 and 3 often used to balance sensitivity and model accuracy. The parameter $r=0.2\times$S.D. (signal standard deviation) was selected in alignment with guidelines that suggest r values between 0.1 and 0.2 times the standard deviation of the signal, providing a robust estimate of entropy while maintaining appropriate discrimination between patterns (Lake et al. 2002; Richman and Moorman 2000). Signal-to-noise ratio (SNR) was calculated using the formula shown in Equation (2).

$$\text{SNR} = 20\log_{10}\frac{\frac{1}{n}\sum^{n}\text{Spike Amplitude}}{\text{Baseline RMS}} \tag{2}$$

The overall data processing workflow is diagrammed in Figure 2.

2.5 | Statistical Methods

Results are reported as mean ± standard deviation. To manage high-frequency data, continuous recordings were segmented into 10-min intervals for processing. Before statistical testing and data visualization, metrics from segmented recordings were aggregated for each subject by the date of recording and the variable under investigation (e.g., light cycle vs. dark cycle) based on the specific hypothesis. For example, the scattered points overlaid on Figure 3a each use an average of 3.5 h of data. This aggregation served to reduce variability and simplify statistical analysis without compromising the fidelity needed to address our hypotheses. To account for variations in recording length, means and variances were weighted by the recording length after denoising. Mixed-effects modeling was used for testing statistical significance. Fixed effects were tested using Satterthwaite's method for degrees of freedom, and post hoc contrasts were performed with estimated marginal means (EMMEANS). A quantitative evaluation of diurnal variations was performed by fitting a cosinor model to data and performing a rhythm detection test (also called the zero-amplitude test) (Cornelissen 2014; Refinetti et al. 2007). The rhythm detection test is an F-ratio calculated using the formula shown in Equation (3).

$$F = \frac{\frac{\sum\left(\hat{Y}_i-\overline{Y}\right)^2}{df_1}}{\frac{\sum\left(Y_i-\overline{Y}\right)^2}{df_2}} \tag{3}$$

where $df_1 = 2$, $df_2 = N\text{-}3$, where $\hat{Y}_i$ is the ith estimated value, Y_i is the ith observed value, $\hat{Y}$ is the arithmetic mean of observed values and N is the number of timepoints (Cornelissen 2014). The zero-amplitude hypothesis was rejected when for $\alpha = 0.05$, $F > F_{1-\alpha}(2, N-3) = 3.00$. All statistical analyses were conducted with R (version 4.4.1).

3 | Results

3.1 | Signal Quality and Stability

Signal-to-noise ratio (SNR) was used to evaluate the quality and stability of neural recordings in the vagus nerve by quantifying the ratio of desired signal-to-background noise. Intraneural CNTY electrodes have demonstrably provided a stable, high SNR interface for chronic recording of ENG signals up to 4 months after implantation (Kotamraju et al. 2023; Marmerstein et al. 2022; McCallum et al. 2017). A high SNR recording from CNTY electrodes is illustrated in Figure 1g, in which spikes were identified using a thresholding algorithm. Figures S2 and S3 show vagus nerve recordings at different time resolutions, highlighting bursting patterns and spiking variations with and without anesthesia. Figure 3 depicts SNR for each subject and over time, and it indicates that SNR for each subject was stable and of high quality (343.8 h from 7 subjects). In Figure 3a, which shows subject-wise SNR variations, the average SNR surpassed 10 dB for each subject. Figure 3b presents SNR fluctuations over an 18-week period post-electrode implantation averaged across all subjects, and it shows that the average SNR was stable and consistently exceeded the 10 dB threshold. Mixed-effects modeling, accounting for random effects of subjects and anesthesia status, indicates that the change in SNR over time was not statistically significant (estimate = 0.02 dB, SE = 0.06 dB, $p = 0.76$). See Figure S4 for additional signal quality and stability measures over time, including spike rate and the peak-to-peak ENG threshold.

3.2 | Effect of Anesthesia on Chronic Vagus Nerve Activity

To determine the effect of anesthesia on vagal activity, we compared vagal neural signals between male Sprague Dawley rats anesthetized with 2% isoflurane and those without anesthesia. After denoising and filtering, 30.5 h of data were collected from 5 anesthetized subjects and 313.2 h of data were collected from 4 non-anesthetized subjects. For 2 of these subjects, recordings were conducted both with and without anesthesia on separate days (i.e., the subjects were common to both groups), resulting in a total of 7 subjects (see Section 2.3 for details). In Figures 4–6, part (a) shows an example of ENG activity with subjects either anesthetized or non-anesthetized, and part (b) magnifies a section of the recordings to highlight differences in signal amplitude and variation. Neural activity was observed in both anesthetized and non-anesthetized subjects, but activity was statistically higher in non-anesthetized subjects when compared with anesthetized subjects.

Neural activity obtained from anesthetized and non-anesthetized subjects is shown in Figure 4a–c. In Figure 4c, the RMS of vagus nerve activity from Figure 4a is depicted with a 50 ms window and a 25 ms overlap. When subjects were not under anesthesia, vagus nerve activity measured by RMS had greater variability and amplitude compared to when subjects were under anesthesia. Figure 4d considers the RMS across all subjects. Normal vagal tone was 6.01 ± 3.36 μV RMS (313.2 h from 4 subjects) and

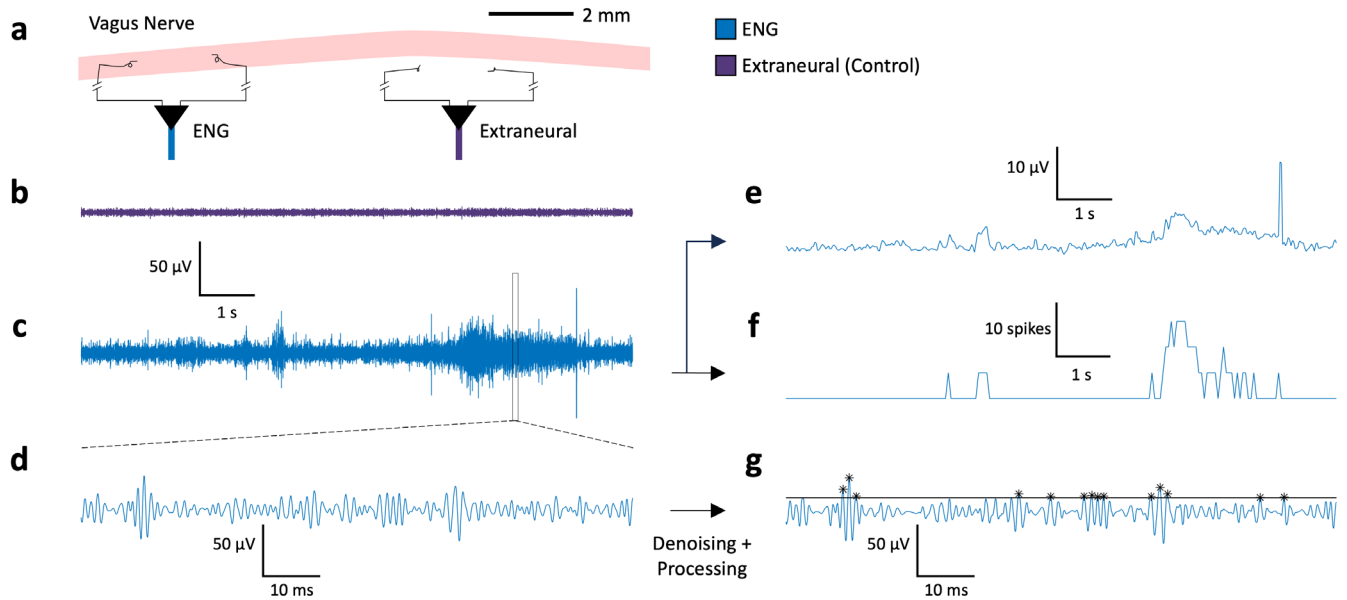

FIGURE 1 | Experimental set-up for neural signal processing. (a) Implantation of carbon nanotube yarn (CNTY) electrodes within and two additional electrodes outside the vagus nerve, with the latter serving as a control during recording sessions to detect common-mode signals. (b) Electrogram traces from extraneural control electrodes displaying background noise. (c) Simultaneous electrogram traces from the vagus nerve revealing pronounced electrical activity. (d) Enlarged segment highlighting nerve activity. (e) RMS of vagus nerve activity with a window of 50 ms and overlap of 25 ms. (f) Vagus spike-rate encoding used for calculating sample entropy. (g) Enlarged segment with noise reduction and identified spikes. The black bar represents the ENG threshold used for spike detection, which is calculated individually for each day and subject.

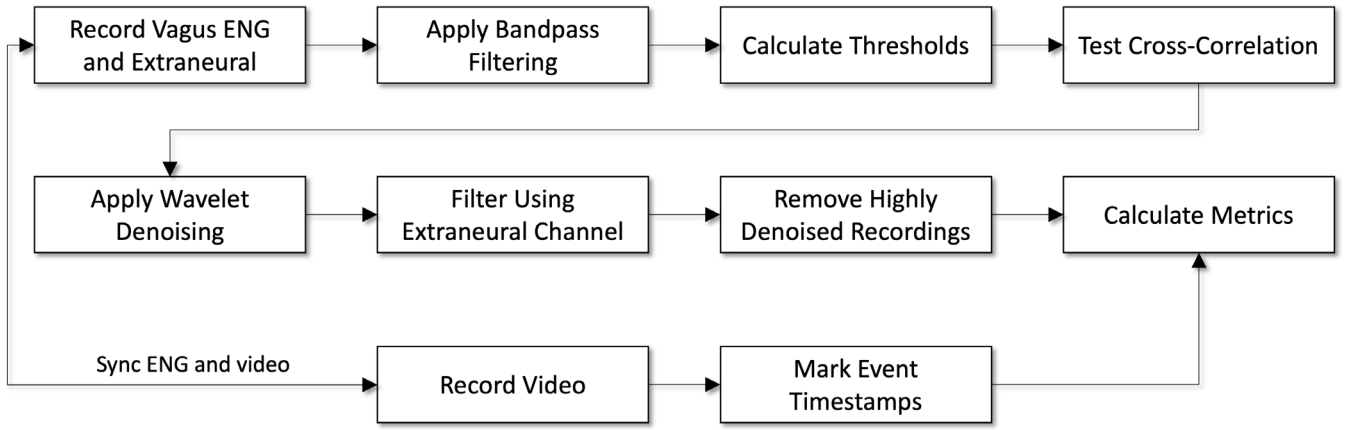

FIGURE 2 | Flowchart of the data processing procedure. The data were sampled continuously at a frequency of 20 kHz with a 5 kHz low-pass filter and segmented into 10-min intervals for processing. A digital 7th order Butterworth bandpass filter [500 Hz, 1200 Hz] was applied to the signals. ENG and extraneural thresholds were determined by multiplying the lowest RMS value within a 10-s window (per subject and day) by a factor of 4.5. ENG and extraneural data with a cross-correlation above 0.3 were filtered out. Sym7 wavelets were employed for wavelet denoising. When extraneural data samples exceeded the extraneural threshold, concurrent ENG data samples were removed. After denoising, recording intervals less than 2 min in length were removed. The metrics signal-to-noise ratio, RMS, spike-rate, and sample entropy were calculated. A video camera manually synced to the ENG recordings was used to determine the first head movement following anesthesia.

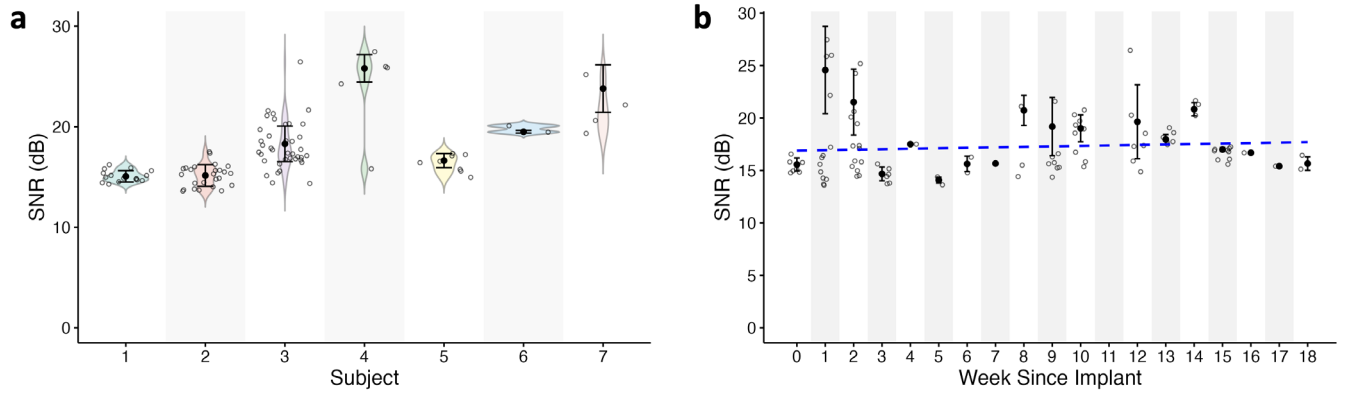

FIGURE 3 | Signal-to-noise ratio (SNR) analysis of detected spikes in chronic recordings. (a) Subject-wise variation in SNR by mean and standard deviation (SD) ($n = 7$). Each data point represents the average SNR of all recordings performed for a given animal on a particular day. (b) Tracking SNR patterns across subjects over weeks since electrode implant by mean and SD, with a dashed blue line indicating the flat trend ($n = 7$). Each data point represents a unique subject and recording date for a given week.

vagal tone under isoflurane anesthesia was $0.93 \pm 0.62\,\mu$V RMS (30.5 h from 5 subjects, with 2 subjects common to both conditions). Data from days involving transitions off anesthesia were excluded from this analysis and are discussed in Section 3.3. Mixed-effects modeling, accounting for random effects of subjects and days since implantation, confirms that anesthesia significantly suppresses vagal RMS (estimate $= -4.25\,\mu$V RMS, SE $= 0.89\,\mu$V RMS, $p < 0.001$).

Figure 5 shows vagus nerve activity measured by spike-rate (Figure 5a–c). As shown in Figure 5c, the number of spikes was significantly higher when subjects were not under anesthesia compared to when they were (detected spikes are indicated by asterisks above the ENG threshold, which is calculated for each day and subject). Figure 5d aggregates this data across all subjects (where spike-rate was calculated as spike count divided by recording length). Normal vagal spike-rate was 128.4 ± 92.8 spikes/s (313.2 h from 4 subjects) and vagal spike-rate under isoflurane anesthesia was 20.7 ± 18.4 spikes/s (30.5 h from 5 subjects, with 2 subjects common to both conditions). Data from days involving transitions off anesthesia were excluded from this analysis and are discussed in Section 3.3. Mixed-effects modeling, accounting for random effects of subjects and days since implantation, confirms that anesthesia significantly suppresses vagal spike-rate (estimate $= -101.8$ spikes/s, SE $= 24.6$ spikes/s, $p < 0.003$).

We next analyzed the sample entropy of the signal in order to assess its information content (Figure 6a–c). To calculate sample entropy, the vagal spike train was encoded into 50 ms bins and spike frequency categories. As shown in Figure 6c, when subjects were not under anesthesia, the spike-rate encoding was significantly more complex than when subjects were under anesthesia. Figure 6d considers the sample

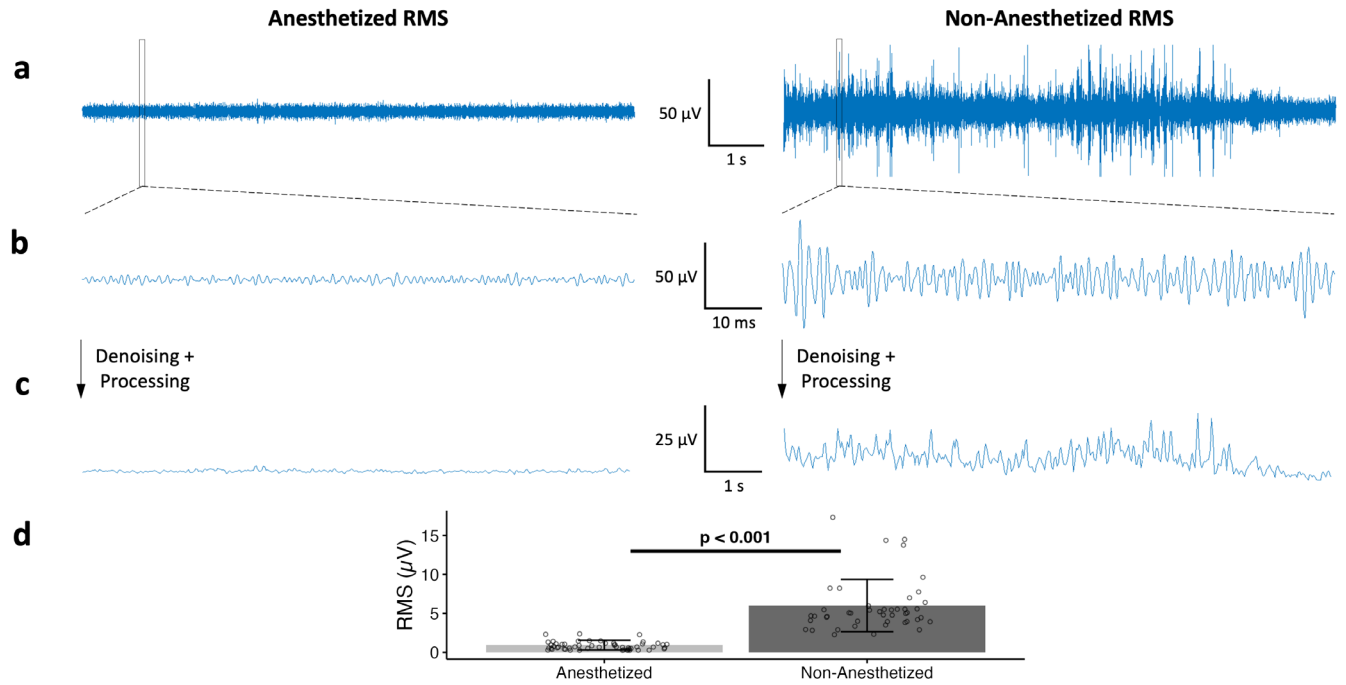

FIGURE 4 | Effect of anesthesia on chronic vagus nerve activity measured by root-mean-square (RMS). (a) Electrogram traces from the vagus nerve revealing pronounced electrical activity. (b) Magnified segment highlighting nerve activity. (c) RMS of denoised vagus nerve activity with a window of 50 ms and overlap of 25 ms. (d) Mean and standard deviation of the vagus nerve RMS by recording. Each data point represents the average RMS of all recordings performed for a given animal on a particular day. RMS was significantly suppressed by anesthesia ($n = 5$ anesthetized, $n = 4$ non-anesthetized, with 2 subjects common to both groups; $p < 0.001$, mixed-effects modeling).

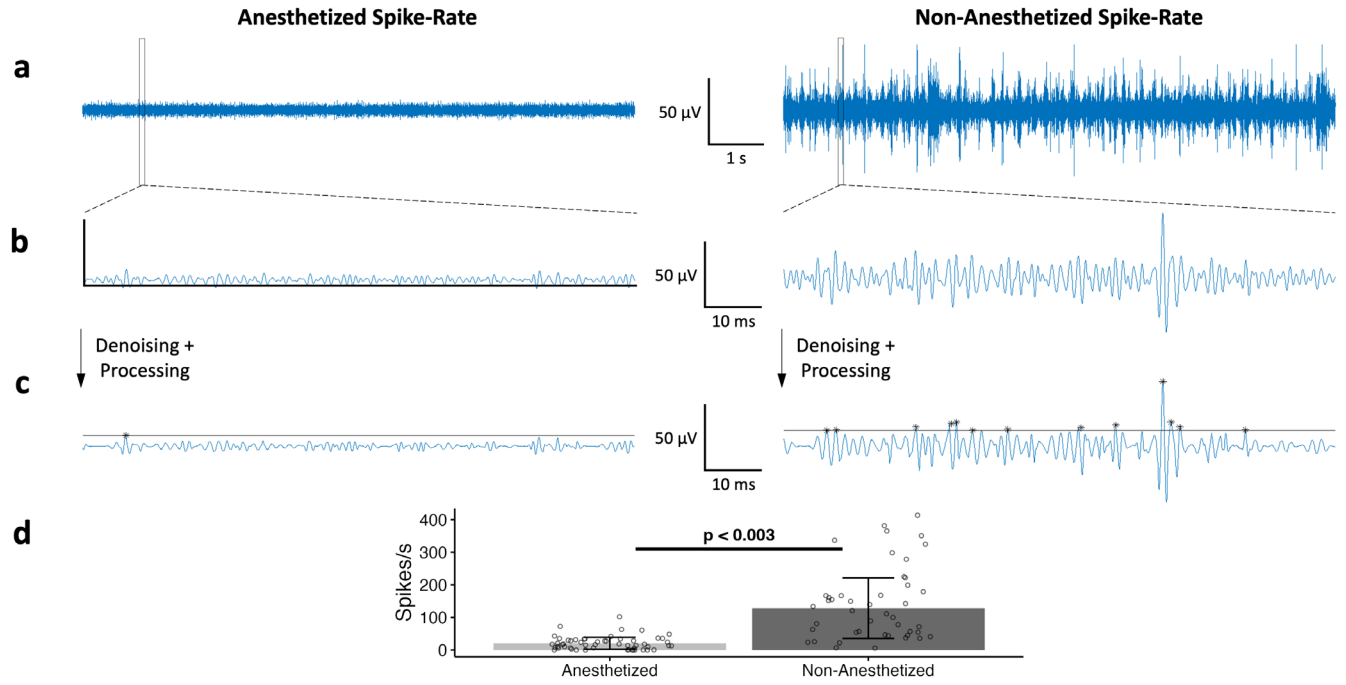

FIGURE 5 | Effect of anesthesia on chronic vagus nerve activity measured by spike-rate. (a) Electrogram traces from the vagus nerve revealing pronounced electrical activity. (b) Magnified segment highlighting nerve activity. (c) Magnified segment with noise reduction and identified spikes. The black bar represents the ENG threshold used for spike detection, which is calculated individually for each day and subject. (d) Mean and standard deviation of the vagus nerve spike-rate by status. Each data point represents the average spike-rate of all recordings performed for a given animal on a particular day. Spike-rate was significantly suppressed by anesthesia ($n = 5$ anesthetized, $n = 4$ non-anesthetized, with 2 subjects common to both groups; $p < 0.003$, mixed-effects modeling).

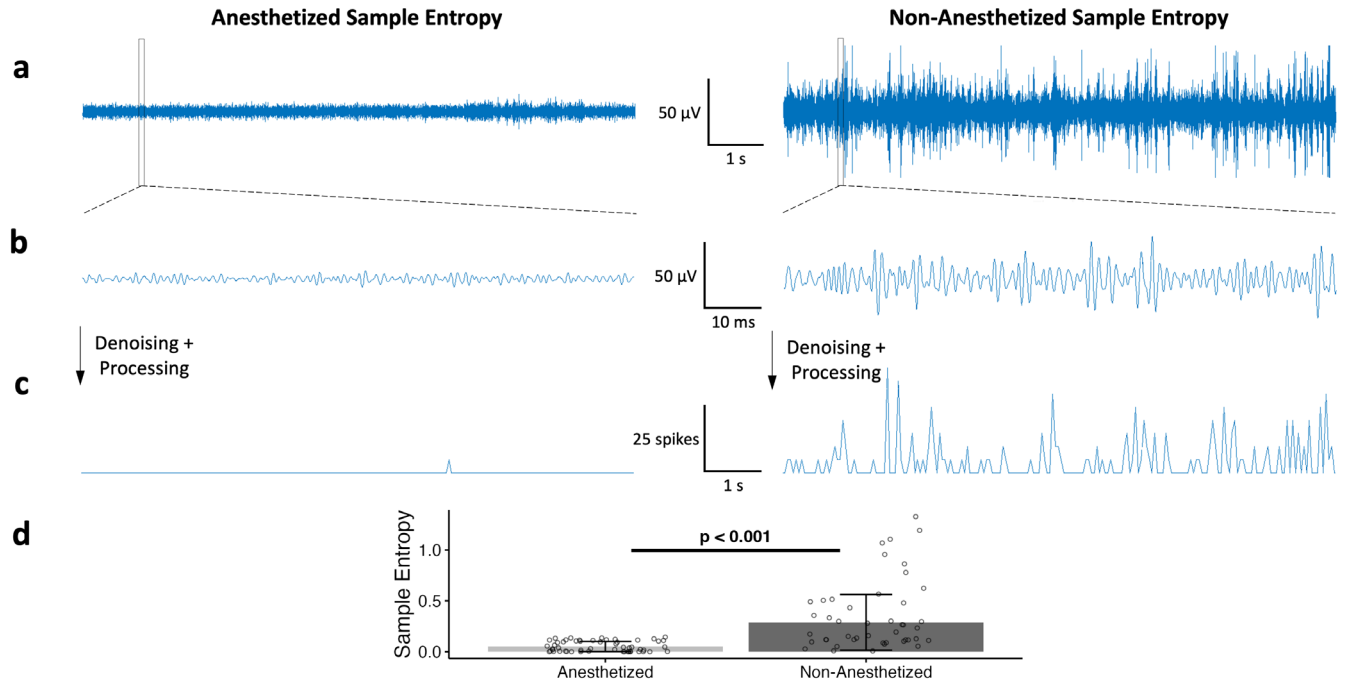

FIGURE 6 | Effect of anesthesia on chronic vagus nerve activity measured by sample entropy. (a) Electrogram traces from the vagus nerve revealing pronounced electrical activity. (b) Magnified segment highlighting nerve activity. (c) Vagus spike-rate encoding used for calculating sample entropy. (d) Mean and standard deviation of the vagus nerve sample entropy by status. Each data point represents the average sample entropy of all recordings performed for a given animal on a particular day. Sample entropy was significantly suppressed by anesthesia ($n = 5$ anesthetized, $n = 4$ non-anesthetized, with 2 subjects common to both groups; $p < 0.001$, mixed-effects modeling).

entropy across all subjects. Normal vagal sample entropy was 0.289 ± 0.273 (313.2 h from 4 subjects) and vagal sample entropy under isoflurane anesthesia was 0.051 ± 0.050 (30.5 h from 5 subjects, with 2 subjects common to both conditions). Data from days involving transitions off anesthesia were excluded from this analysis and are discussed in Section 3.3. Mixed-effects modeling, accounting for random effects of subjects and days since implantation, confirms that anesthesia significantly suppresses vagal spike train complexity (estimate $= -0.297$, SE $= 0.048$, $p < 0.001$).

3.3 | Effect of Terminating Anesthesia on Chronic Vagus Nerve Activity

To study vagal activity during the transition from anesthesia to wakefulness, male Sprague Dawley rats were taken off 2% isoflurane anesthesia while recording. After denoising and filtering, 89.8 h of data were collected from 5 subjects during recovery from anesthesia. These data are independent of the data analyzed in Figures 4–6.

Figure 7 shows the gradual effect of terminating 2% isoflurane on vagus nerve spike rate (52.7 h from 7 subjects). Figure 7a displays the mean and standard deviation (SD) of vagus nerve spike rate segmented into 30-min intervals. Time zero designates the time of initial subject head movement following the termination of anesthesia supply; head movement usually preceded full-body movement and alertness and was used to demarcate initial recovery. See Figure S5 for the immediate effect of terminating 2% isoflurane, which aligns with Figure 7a and uses the point at which anesthesia supply was terminated as a reference for time zero. Figure S5 shows a brief peak in vagal activity around 10 min, consistent with righting reflex recovery, while Figure 7 highlights the sustained suppression and gradual recovery over 2 h. From the recordings, we observed that subject head movement occurred 12.5 ± 0.9 min following the termination of anesthesia. Figure 7a shows the neural activity during three phases: anesthesia (red line), recovery (purple line), and stability (blue line). The results indicate that the spike rate recovers steadily for 2 h after observed subject movement. Figure 7b compares the average spike rate before head movement and 2 h after head movement. Across all subjects, vagal spike rate before head movement was 21.1 ± 29.5 spikes/s (4.7 h from 7 subjects) and vagal spike rate within 2 to 5 h after head movement was 83.7 ± 72.0 spikes/s (20.0 h from 4 subjects). Mixed-effects modeling, accounting for random effects of subjects and days since implantation, confirms that this difference in spike rate is statistically significant (estimate $= -80.8$ spikes/s, SE $= 27.7$ spikes/s, $p < 0.02$). In addition, when the spike rate within 2 to 5 h after head movement was compared to data from behaving, non-anesthetized subjects during daytime (see Figure 9d), the difference was not statistically significant (estimate $= -29.9$ spikes/s, SE $= 28.4$ spikes/s, $p = 0.55$). Normal daytime activity was used as the benchmark for recovery and normal activity because anesthesia termination tests were done during daytime (see Figure 8). In addition, diurnal variations play a significant role in characterizing vagal activity (see Figures 8 and 9). Overall, the data show that anesthesia significantly suppresses vagal tone at least 2 h past the end of its administration.

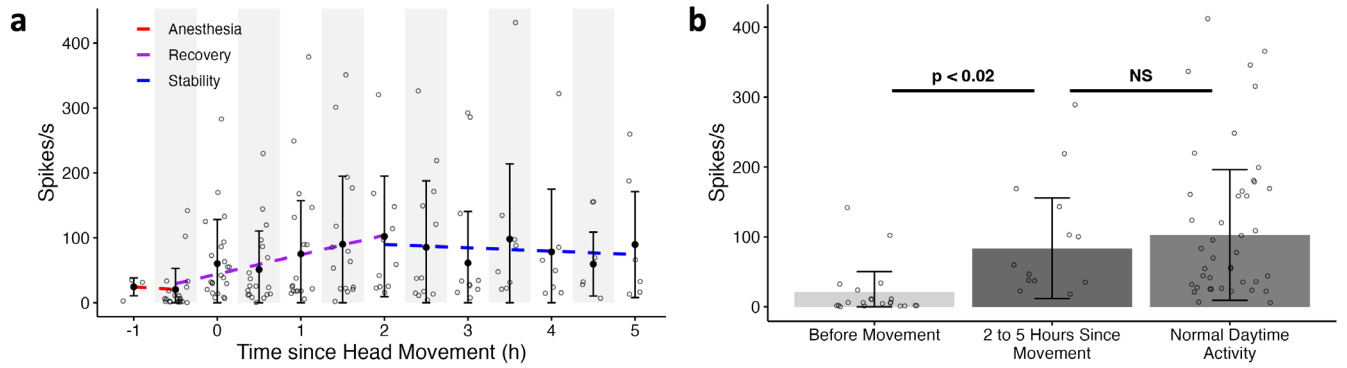

FIGURE 7 | Effect of terminating anesthesia on spike-rate. (a) Mean and standard deviation of the vagus nerve spike-rate. Spike-rate is presented in 30-min intervals, with 0 demarcating the time of subject head movement following anesthesia supply termination ($n = 7$). Each data point represents the average spike-rate for all recordings performed for a given animal during a 30-min interval. The three observed phases are anesthesia (red line), recovery (purple line), and stability (blue line). (b) Mean and standard deviation of the vagus nerve spike-rate. Each data point represents the average spike-rate for all recordings performed for a given animal during a specific time interval. Vagus nerve activity is significantly higher 2 h after initial subject head movement ($n = 7$, $p < 0.02$, mixed-effects modeling).

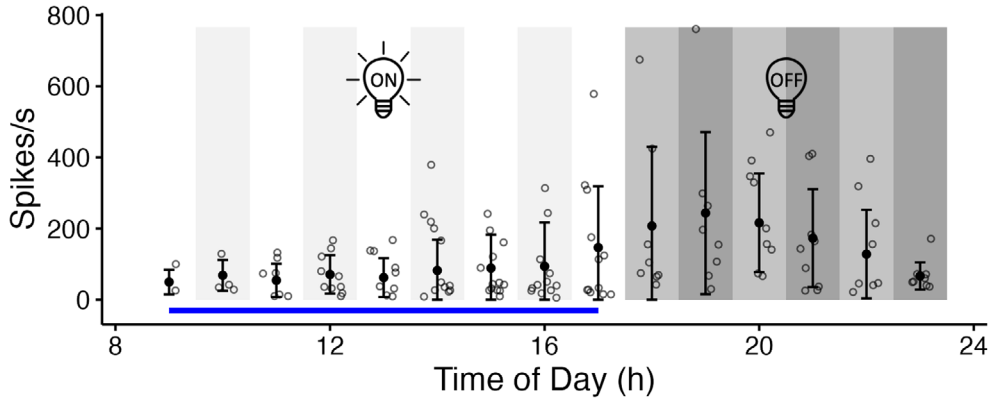

FIGURE 8 | Recovery from anesthesia does not affect diurnal variations by hourly spike-rate ($n = 7$). Mean and standard deviation of the vagus nerve spike-rate after uniformly distributed wakeup events. Each data point represents the average spike-rate for all recordings performed for a given animal during a 1-h interval. The light and dark backgrounds correspond to the light and dark cycles in the animal facility, respectively. The blue bar indicates the period in which wakeup events occurred. Regardless of the timing of wakeup events, the average spike-rate exhibits a discernible diurnal pattern across the time of day.

To better understand the lasting effect of anesthesia on vagal tone, Figure 8 considers the average spike rate by the hour of day, on the days when subjects were taken off anesthesia (89.8 h from 7 subjects). Whereas Figure 7 considers data up to 5 h after anesthesia was terminated, Figure 8 considers spike rate variations throughout the time of day irrespective of when anesthesia was terminated. Subjects were taken off anesthesia at random times during the daytime. The dark background in Figure 8 corresponds to the time when lights are off in the animal care facility (6:00 pm to 6:00 am). The increase in spike rate extending into the dark cycle suggests that there are diurnal variations to vagus nerve activity and that these diurnal variations are not significantly affected by anesthesia recovery.

3.4 | Effect of Diurnal Variations on Chronic Vagus Nerve Activity

Diurnal variations are also known to affect the amplitude of vagus nerve activity (Smets et al. 2022). In order to compare the effect of anesthesia and diurnal variations on the vagus nerve activity, experiments were carried out with nonanesthetized freely behaving male Sprague Dawley rats. After denoising and filtering, 313.2 h of data were collected from 4 subjects.

Figure 9 presents vagal activity during the light and dark cycles for non-anesthetized subjects. Figure 9a shows an example of ENG activity during light (day) and dark (night) cycles in the animal care facility, and Figure 9b magnifies a section of the recordings to highlight differences in signal amplitude and variation. As shown in Figure 9c, during the dark cycle, the number of spikes is significantly greater than during the light cycle (detected spikes are indicated by asterisks above the ENG threshold, which is calculated for the entire day per subject). Figure 9d shows the average spike rate by the hour of day, and Figure 9e compares the spike rate between light and dark cycles (313.2 h from 4 subjects). Figure 9d–gdisplay the spike rate across all non-anesthetized subjects. Vagal spike rate was 102.7 ± 93.5 spikes/s during the light cycle and 152.9 ± 94.8 spikes/s during the

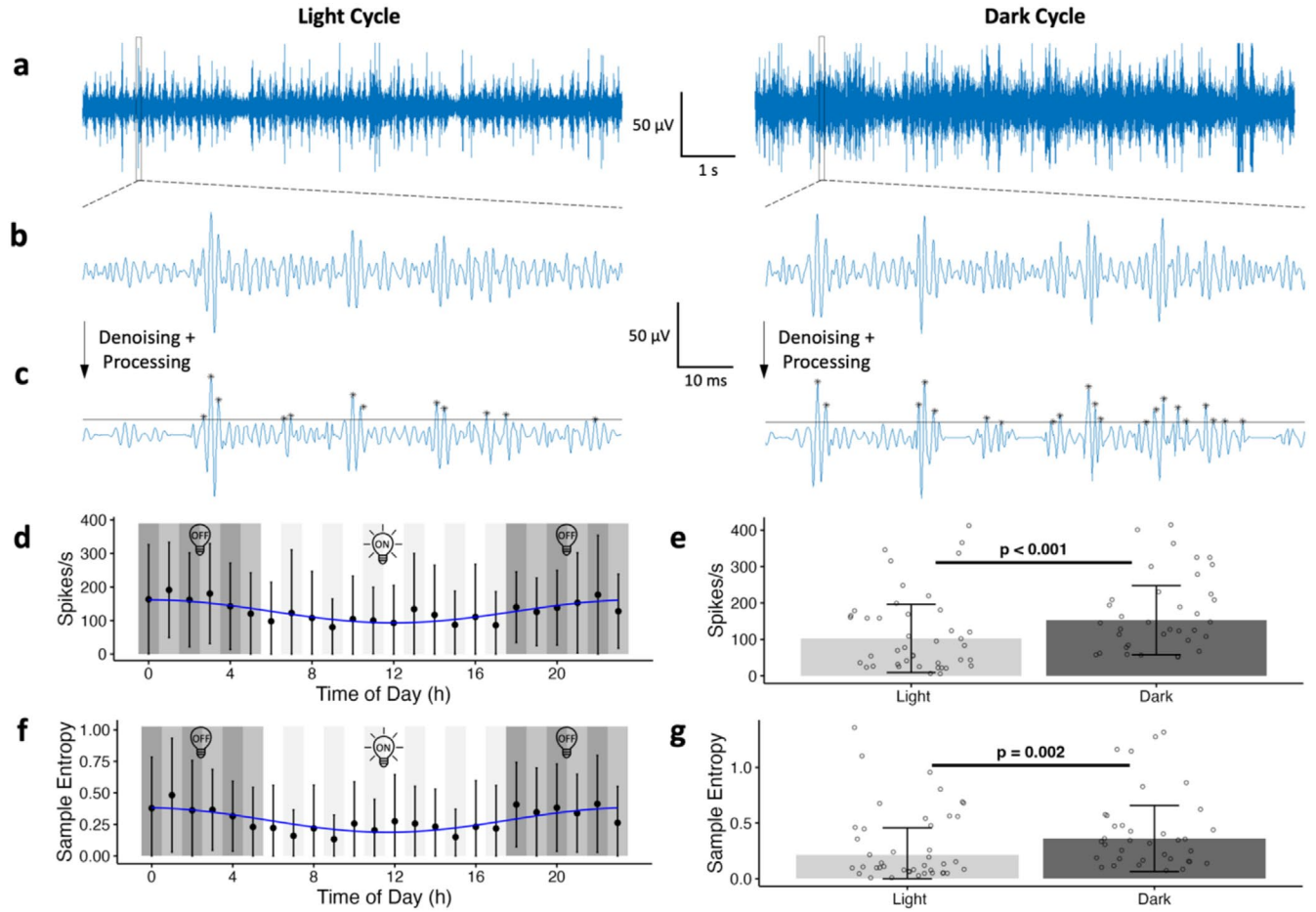

FIGURE 9 | Hourly spike-rate variation. (a) Electrogram traces from the vagus nerve revealing pronounced electrical activity. (b) Magnified segment highlighting nerve activity. (c) Magnified segment with noise reduction and identified spikes. The black bar represents the ENG threshold used for spike detection, which is calculated individually for each day and subject. (d) The mean and standard deviation (SD) of vagus nerve spike-rate exhibits a discernible diurnal pattern across a 24-h period ($n = 4$). The light and dark backgrounds correspond to the light and dark cycles in the animal facility, respectively. The blue wave represents the cosine wave best fit to the data. (e) Mean and SD of the vagus nerve spike-rate between light and dark cycles in the animal facility ($n = 4$, $p < 0.001$, mixed-effects modeling). Each data point represents the average spike-rate for all recordings performed for a given subject during a 1-h interval. (f) The mean and SD of vagus nerve sample entropy exhibits a discernible diurnal pattern across a 24-h period ($n = 4$). Light and dark cycles in the animal facility and the cosine wave best fit to the data are included. (g) Mean and SD of the vagus nerve sample entropy between light and dark cycles in the animal facility ($n = 4$, $p = 0.002$, mixed-effects modeling). Each data point represents the average sample entropy for all recordings performed for a given subject during a 1-h interval.

dark cycle. Mixed-effects modeling, accounting for random effects of subjects and days since implantation, confirms that vagal spike rate is significantly greater during the dark cycles (estimate = −44.5 spikes/s, SE = 12.2 spikes/s, $p < 0.001$). Additionally, a cosinor test shows that there is a significant diurnal pattern in vagal spike rate across the 24-h cycle (df = 540, $F = 17.3$, $p < 0.001$). Figure 9f shows the average sample entropy by the hour of day, while Figure 9g compares the sample entropy between light and dark cycles (313.2 h from 4 subjects). To calculate sample entropy, the vagal spike train was encoded into 50 ms bins and spike frequency categories. During light cycles, vagal sample entropy was 0.213 ± 0.244, and during dark cycles, vagal sample entropy was 0.361 ± 0.297. Mixed-effects modeling, accounting for random effects of subjects and days since implantation, confirms that vagal spike train complexity is significantly greater during the dark cycles (estimate = −0.096, SE = 0.029, $p = 0.002$). Additionally, a cosinor test shows that there is a significant diurnal pattern in vagal sample entropy across the 24-h cycle (df = 540, $F = 14.4$, $p < 0.001$). These data suggest that diurnal variations play a significant role in vagus nerve activity.

Importantly, the decrease in vagal activity during anesthesia is significantly higher than the natural decrease during the light cycle. When comparing information from Sections 3.2 and 3.4, mixed-effects modeling shows that anesthesia significantly suppresses vagal activity compared to light cycle recordings for both spike-rate (estimate = −106.6 spikes/s, SE = 21.4 spikes/s, $p = 0.030$) and sample entropy (estimate = −0.243, SE = 0.045, $p < 0.001$). Taken together, these results show the pronounced inhibitory effect of anesthesia on vagal activity, indicating its dominance over diurnal modulation.

4 | Discussion

This is the first study of vagal activity and anesthesia that recorded direct vagus nerve activity from non-anesthetized subjects, and we have provided evidence that anesthesia with 2% isoflurane suppresses vagus nerve activity. While previous research has primarily relied on indirect measures, such as heart rate variability (Bouairi et al. 2004; Chapleau and Sabharwal 2011; Halliwill and Billman 1992; Picker et al. 2001), our approach employed novel chronic, differential recording techniques to directly record vagus nerve activity in non-anesthetized subjects (Figure 1).

Custom ultra-low noise electronics (Dweiri et al. 2015), which included intraneural and extraneural CNTY differential electrodes, were used to establish a stable, high SNR interface (Figure 3). Rigorous signal processing methods mitigated motion artifacts and enabled careful analysis of freely moving and anesthetized subjects (Figure 2). Vagus nerve activity fluctuates significantly over short time spans—for example, freely moving rats go through eating, grooming, and resting states that significantly affect vagus nerve activity (Marmerstein et al. 2022). Given that our hypotheses focus on longer time intervals (e.g., anesthesia effects or diurnal variations), we performed binning at appropriate resolutions based on the specific hypothesis (e.g., 24-h aggregates for chronic SNR analysis or 30-min bins for recovery dynamics). This aggregation served to reduce variability and simplify statistical analysis without compromising the fidelity needed to address our hypotheses. Additionally, the information theory metrics used in this study can be applied to shorter time bins during feature selection for classification of different neuronal subtypes, as demonstrated by Marmerstein et al. (2022).

This study included only male subjects, which is a limitation of this study. Although the decision was made to reduce potential variability from sex differences, emerging evidence indicates that male and female animals respond differently to isoflurane anesthesia, mediated by hormonal pathways. Testosterone influences neurotransmitter systems, affecting anesthetic depth and prolonging recovery times in males, while estrogen receptor-alpha modulates anesthetic effects in females (Wasilczuk et al. 2024; Zhang et al. 2022). Additionally, sex differences in circadian rhythms are well documented and could influence light/dark variations in vagus nerve activity (Krizo and Mintz 2015). Future studies investigating these differences in male and female animals would provide valuable insights into the interplay between anesthesia, diurnal variations, and vagus nerve activity.

The inhibitory effect of isoflurane anesthesia on the vagus nerve observed in this study aligns with the results of previous studies (Bouairi et al. 2004; Chapleau and Sabharwal 2011; Halliwill and Billman 1992; Kato et al. 1992; Picker et al. 2001; Silverman et al. 2018). Silverman et al. (2018) compared direct baseline vagus nerve activity between different isoflurane levels and found that spike count at 1.5% isoflurane was significantly greater than spike count at 2.0% isoflurane, which suggests that lower isoflurane levels can reduce the effect of anesthesia on the vagus nerve. Because the technology for recording direct vagus nerve activity is nascent, most related studies on the impact of anesthesia on vagus nerve activity use heart rate and HRV as an alternative measure, which refers only to efferent vagal activity. Multiple studies have observed increased heart rate (Bouairi et al. 2004; Chapleau and Sabharwal 2011; Halliwill and Billman 1992; Picker et al. 2001) and reduced HRV (Kato et al. 1992; Picker et al. 2001) during anesthesia, which is consistent with our finding that anesthesia inhibits vagus nerve activity.

Our study used the metrics RMS, spike-rate, and sample entropy to characterize the inhibitory effect of isoflurane on vagus nerve activity. The significant reduction in RMS (Figure 4), spike-rate (Figure 5), and sample entropy (Figure 6) during anesthesia suggests that anesthesia decreases information content in the vagus nerve. The novel use of sample entropy is of particular interest, as it encodes spike trains into a quantitative measure of the randomness or complexity of the vagus nerve activity, which is related to its information content (Delgado-Bonal and Marshak 2019). The significant reduction in sample entropy during anesthesia indicates a shift toward a more predictable and less complex neural pattern in the vagus nerve. Sample entropy was introduced by Richman and Moorman, who found it to be a more suitable measure than approximate entropy for noisy biological time series data (Richman and Moorman 2000). Although sample entropy has been used for assessing information content in HRV (Lake et al. 2002; Yan et al. 2022), it has not previously been used in the analysis of peripheral nervous system (PNS) spike trains (Bialek et al. 1991; Borst and Theunissen 1999; Nemenman et al. 2004; Rieke et al. 1999). Recently, information theory measures such as Shannon entropy have been applied to PNS neural data analysis (Kotamraju et al. 2023), which suggests that there is growing interest in quantifying information content and complexity in peripheral nerve signals. Strong et al. explored the concept of entropy in neural spike trains, offering insight into the limitations of entropy estimation when binning and selecting a time resolution. This binned approach to entropy estimation aligns with our own, although a binless approach that embeds spike trains into vector spaces and entropy estimates based on nearest-neighbor Euclidean distances has been proposed by Victor (2002). Future studies may find that the use of sample entropy for entropy approximation of vagus nerve activity complements other approximation methods, such as Shannon entropy (Kotamraju et al. 2023; Nagaraj and Balasubramanian 2017; Paninski 2003) or Lempel-Ziv complexity (Aboy et al. 2006; Amigó et al. 2004; Nagaraj and Balasubramanian 2017).

In this study, we have also provided evidence that anesthesia with 2% isoflurane suppresses vagus nerve activity for up to 2 h past its administration (Figure 7). Early studies on isoflurane recovery observed rapid elimination, with patients regaining consciousness within approximately 10 min after significant exposure (Cromwell et al. 1971; Eger 1981). Our observations and other studies identified a similar recovery pattern in rats, with recovery typically lasting around 10 min as measured by the return of the righting reflex (Miller et al. 2016; Sinon et al. 2021; Wang et al. 2014). Our findings suggest that the effect of isoflurane anesthesia on the vagus nerve extends beyond the observed recovery point, continuing for over 2 h after terminating isoflurane delivery. This delayed vagal recovery may reflect broader nervous system effects of isoflurane, such as its impact on neurotransmitter systems involved in autonomic regulation

and circadian rhythms (Sugano et al. 2021). Additionally, these effects align with a study reporting reduced vagal activity during isoflurane recovery (Falcone et al. 2020). To our knowledge, the prolonged residual effects of anesthesia on vagus nerve activity have not been reported before. However, the potential for chronic recording of vagus nerve activity during anesthesia could significantly improve our understanding of how to maintain adequate levels of anesthetics in the presence of a significantly decreased amount of information to the brain, which would aid in maintaining homeostasis.

Although the biochemical mechanisms underlying the effect of isoflurane anesthesia on vagus nerve activity are complex, previous studies offer valuable insights. Isoflurane predominantly acts via the $GABA_A$ receptor in neocortical neurons (Antkowiak 1999; Caraiscos et al. 2004; Jenkins et al. 2001), and $GABA_A$ receptors regulate vagal activity in the dorsal motor nucleus of the vagus (Gao and Smith 2010). GABAergic neurons in the nucleus ambiguus control parasympathetic vagal activity, and activation of $GABA_A$ receptors inhibits vagal tone (Bentzen and Grunnet 2011). Consequently, anesthesia-induced modulation of $GABA_A$ receptors likely contributed to the observed reduction in vagus nerve activity. Another mechanism by which anesthesia inhibits vagus nerve activity involves the suppression of neuronal activity in the brainstem. Leung and Mason (1995) showed that at concentrations of isoflurane ranging from 1.7% to 1.9% in rats, inhibitory output neurons in the pontomedullary raphe magnus and nucleus reticularis paragigantocellularis pars α are not activated. An additional example of isoflurane inhibiting nerve activity is one study which found that isoflurane augmented inhibitory transmission mediated by γ-aminobutyric acid, leading to a decrease in the excitability of spinal dorsal horn neurons (Wakai et al. 2005). Although the precise mechanism of prolonged vagal suppression despite behavioral recovery is not known, several factors may contribute. Field et al. (2021) demonstrated that $GABA_A$ receptor desensitization can trigger long-term potentiation at inhibitory synapses lasting up to 24 h. Magnuson et al. (2014) reported that in rats receiving 30 min of 2% isoflurane before switching to dexmedetomidine, alterations in functional connectivity persisted for up to 2.75 h, indicating a sustained impact on neural activity. Bárez-López et al. (2023) showed that isoflurane rapidly induces region-specific phosphorylation modifications affecting proteins involved in synaptic signaling, which suggests that post-translational modifications in autonomic regulatory centers could sustain vagal suppression well after the anesthetic has been metabolized. Isoflurane also reduces neural excitability by inhibiting Ca^{2+} and Na^{+} channels essential for the generation and propagation of action potentials (Hirota et al. 1999; Kameyama et al. 1999; Ouyang and Hemmings 2005; Wu et al. 2004).

We observed a significant diurnal pattern in the vagus nerve activity of behaving, non-anesthetized subjects (Figure 9e,g). Characterizing the diurnal variations of vagal tone is of significant interest, as it sheds insight into the temporal patterns of autonomic nervous system activity and the optimal times for treatments targeting vagal modulation. For example, circadian rhythms profoundly influence seizure susceptibility (Quigg 2000), so understanding the effect of diurnal variations in vagus nerve activity may significantly impact epilepsy treatment using vagus nerve stimulation and lead to more targeted treatments. This reasoning extends to other diseases known to be related to the vagus nerve and affected by circadian rhythm, such as obesity (Browning et al. 2017; Froy 2010), depression (Breit et al. 2018; Germain and Kupfer 2008), and cardiovascular control (Browning et al. 2017; Guo and Stein 2003; Wagner 2022).

Although parasympathetic activity, including vagal tone, is conventionally associated with resting states such as the light phase in rats, our findings indicate higher vagal activity during the dark phase, when rats are typically more active. This suggests that behavioral states, such as increased feeding or exploratory activity during the dark phase, may drive vagal tone independently of the rest-activity cycle. Alternatively, the observed pattern may reflect a compensatory response to heightened sympathetic drive during active periods to maintain autonomic balance. These findings highlight the complex interplay between autonomic branches, with direct nerve recordings offering a clearer picture of diurnal vagal patterns compared to traditional HRV measures (Burgess et al. 1997; Li et al. 2011; Makino et al. 1997; Morrison and Pearson 1989; Oosting et al. 1997; Tavakkolizadeh et al. 2005). Our findings are concordant with those of Smets et al. and suggest that there is a significant correlation between vagus nerve activity and diurnal variations (Smets et al. 2022), which an older study using ambulatory dogs was unable to identify (Ogawa et al. 2007). While the observed data exhibit a pattern consistent with circadian rhythms, further controlled studies are needed to fully confirm this association.

Overall, this study utilized chronic, differential recording techniques to investigate the impact of 2% isoflurane anesthesia on vagus nerve activity. The findings reveal a suppression of vagus nerve activity during anesthesia, with significant reductions in RMS, spike rate, and sample entropy. Notably, the use of sample entropy provided insights into the shift toward a more predictable and less complex neural pattern during anesthesia. Additionally, the study demonstrated residual effects persisting over 2 h post-anesthesia and examined the significant correlation between vagus nerve activity and diurnal variations. These results demonstrate the profound impact of anesthesia on vagal activity, suggesting that since 80% of the vagal fibers are afferent, input information to the brain during anesthesia is severely diminished.

Declaration of Transparency

The authors, reviewers and editors affirm that in accordance to the policies set by the *Journal of Neuroscience Research*, this manuscript presents an accurate and transparent account of the study being reported and that all critical details describing the methods and results are present.

Author Contributions

Conceptualization, A.J.R., J.T.M., B.P.K., G.A.M., and D.M.D.; methodology, J.T.M., G.A.M., and D.M.D.; software, A.J.R. and J.T.M.; validation, A.J.R., J.T.M., B.P.K., and G.A.M.; formal analysis, A.J.R.; investigation, J.T.M.; resources, D.M.D.; data curation, A.J.R., J.T.M., and G.A.M.; writing – original draft preparation, A.J.R.; writing – review and editing, B.P.K., J.T.M., G.A.M., and D.M.D.; visualization,

A.J.R.; supervision, G.A.M. and D.M.D.; project administration, D.M.D.; funding acquisition, D.M.D.

Acknowledgments

This work was funded by the National Institutes of Health (Nerve reshaping for improved selectivity, 5R01NS032845-22). Special thanks to William Marcus, who helped monitor animals during surgery and recovery and assisted with recording. This work made use of the High Performance Computing Resource in the Core Facility for Advanced Research Computing at Case Western Reserve University.

Disclosure

Declaration of Generative AI and AI-Assisted Technologies in the Writing Process: During the preparation of this work, the authors used ChatGPT in order to address grammatical issues. After using this tool/service, the authors reviewed and edited the content as needed and took full responsibility for the content of the published article.

Ethics Statement

Institutional Review Board Statement: All surgical and experimental procedures were carried out with the approval and oversight of the Case Western Reserve University Institutional Animal Care and Use Committee to ensure compliance with all federal, state, and local animal welfare laws and regulations (protocol 2016-0328). This study was carried out in compliance with the ARRIVE guidelines.

Conflicts of Interest

The authors declare no conflicts of interest.

Data Availability Statement

Data associated with this study are available through the SPARC Portal (RRID: SCR_017041) under a CC-BY-4.0 license (Marmerstein et al. 2023). All data recorded and the code used for analysis in this study are available upon reasonable request from the corresponding author.

References

Aboy, M., R. Hornero, D. Abasolo, and D. Alvarez. 2006. "Interpretation of the Lempel-Ziv Complexity Measure in the Context of Biomedical Signal Analysis." *IEEE Transactions on Biomedical Engineering* 53: 2282–2288. https://doi.org/10.1109/TBME.2006.883696.

Ahmed, U., Y.-C. Chang, M. F. Lopez, et al. 2021. "Implant- and Anesthesia-Related Factors Affecting Cardiopulmonary Threshold Intensities for Vagus Nerve Stimulation." *Journal of Neural Engineering* 18: 046075. https://doi.org/10.1088/1741-2552/ac048a.

Amigó, J. M., J. Szczepański, E. Wajnryb, and M. V. Sanchez-Vives. 2004. "Estimating the Entropy Rate of Spike Trains via Lempel-Ziv Complexity." *Neural Computation* 16: 717–736. https://doi.org/10.1162/089976604322860677.

Antkowiak, B. 1999. "Different Actions of General Anesthetics on the Firing Patterns of Neocortical Neurons Mediated by the GABAAReceptor." *Anesthesiology* 91: 500–511. https://doi.org/10.1097/00000542-199908000-00025.

Bando, H., T. Nishio, G. T. J. Van Der Horst, S. Masubuchi, Y. Hisa, and H. Okamura. 2007. "Vagal Regulation of Respiratory Clocks in Mice." *Journal of Neuroscience* 27: 4359–4365. https://doi.org/10.1523/JNEUROSCI.4131-06.2007.

Bárez-López, S., G. J. Gadd, A. G. Pauža, D. Murphy, and M. P. Greenwood. 2023. "Isoflurane Rapidly Modifies Synaptic and Cytoskeletal Phosphoproteomes of the Supraoptic Nucleus of the Hypothalamus and the Cortex." *Neuroendocrinology* 113: 1008–1023. https://doi.org/10.1159/000531352.

Bentzen, B. H., and M. Grunnet. 2011. "Central and Peripheral GABAA Receptor Regulation of the Heart Rate Depends on the Conscious State of the Animal." *Advances in Pharmacological Sciences* 2011: 1–10. https://doi.org/10.1155/2011/578273.

Berthoud, H.-R., and W. L. Neuhuber. 2000. "Functional and Chemical Anatomy of the Afferent Vagal System." *Autonomic Neuroscience* 85: 1–17. https://doi.org/10.1016/S1566-0702(00)00215-0.

Bialek, W., F. Rieke, R. R. de Ruyter van Steveninck, and D. Warland. 1991. "Reading a Neural Code." *Science* 252: 1854–1857. https://doi.org/10.1126/science.2063199.

Black, N., A. D'Souza, Y. Wang, et al. 2019. "Circadian Rhythm of Cardiac Electrophysiology, Arrhythmogenesis, and the Underlying Mechanisms." *Heart Rhythm* 16: 298–307. https://doi.org/10.1016/j.hrthm.2018.08.026.

Borst, A., and F. E. Theunissen. 1999. "Information Theory and Neural Coding." *Nature Neuroscience* 2: 947–957. https://doi.org/10.1038/14731.

Bouairi, E., R. Neff, C. Evans, A. Gold, M. C. Andresen, and D. Mendelowitz. 2004. "Respiratory Sinus Arrhythmia in Freely Moving and Anesthetized Rats." *Journal of Applied Physiology (Bethesda, MD: 1985)* 97: 1431–1436. https://doi.org/10.1152/japplphysiol.00277.2004.

Breit, S., A. Kupferberg, G. Rogler, and G. Hasler. 2018. "Vagus Nerve as Modulator of the Brain-Gut Axis in Psychiatric and Inflammatory Disorders." *Frontiers in Psychiatry* 9: 44. https://doi.org/10.3389/fpsyt.2018.00044.

Browning, K. N., S. Verheijden, and G. E. Boeckxstaens. 2017. "The Vagus Nerve in Appetite Regulation, Mood, and Intestinal Inflammation." *Gastroenterology* 152: 730–744. https://doi.org/10.1053/j.gastro.2016.10.046.

Burgess, H. J., J. Trinder, Y. Kim, and D. Luke. 1997. "Sleep and Circadian Influences on Cardiac Autonomic Nervous System Activity." *American Journal of Physiology* 273: H1761–H1768. https://doi.org/10.1152/ajpheart.1997.273.4.H1761.

Caraiscos, V. B., J. G. Newell, K. E. You-Ten, et al. 2004. "Selective Enhancement of Tonic GABAergic Inhibition in Murine Hippocampal Neurons by Low Concentrations of the Volatile Anesthetic Isoflurane." *Journal of Neuroscience* 24: 8454–8458. https://doi.org/10.1523/JNEUROSCI.2063-04.2004.

Chapleau, M. W., and R. Sabharwal. 2011. "Methods of Assessing Vagus Nerve Activity and Reflexes." *Heart Failure Reviews* 16: 109–127. https://doi.org/10.1007/s10741-010-9174-6.

Cohen, J. 1988. *Statistical Power Analysis for the Behavioral Sciences*. 2nd ed. L. Erlbaum Associates.

Cornelissen, G. 2014. "Cosinor-Based Rhythmometry." *Theoretical Biology & Medical Modelling* 11: 16. https://doi.org/10.1186/1742-4682-11-16.

Cracchiolo, M., M. M. Ottaviani, A. Panarese, et al. 2021. "Bioelectronic Medicine for the Autonomic Nervous System: Clinical Applications and Perspectives." *Journal of Neural Engineering* 18: 041002. https://doi.org/10.1088/1741-2552/abe6b9.

Cromwell, T. H., E. I. Eger, W. C. Stevens, and W. M. Dolan. 1971. "Forane Uptake, Excretion, and Blood Solubility in Man." *Anesthesiology* 35: 401–408. https://doi.org/10.1097/00000542-197110000-00017.

Delgado-Bonal, A., and A. Marshak. 2019. "Approximate Entropy and Sample Entropy: A Comprehensive Tutorial." *Entropy* 21: 541. https://doi.org/10.3390/e21060541.

Diedrich, A., W. Charoensuk, R. J. Brychta, A. C. Ertl, and R. Shiavi. 2003. "Analysis of Raw Microneurographic Recordings Based on Wavelet de-Noising Technique and Classification Algorithm: Wavelet

Analysis in Microneurography." *IEEE Transactions on Biomedical Engineering* 50: 41–50. https://doi.org/10.1109/TBME.2002.807323.

Dweiri, Y. M., T. Eggers, G. McCallum, and D. M. Durand. 2015. "Ultra-Low Noise Miniaturized Neural Amplifier With Hardware Averaging." *Journal of Neural Engineering* 12: 046024. https://doi.org/10.1088/1741-2560/12/4/046024.

Eger, E. I. 1981. "Isoflurane." *Anesthesiology* 55: 559–576. https://doi.org/10.1097/00000542-198111000-00014.

Falcone, J. D., T. Liu, L. Goldman, et al. 2020. "A Novel Microwire Interface for Small Diameter Peripheral Nerves in a Chronic, Awake Murine Model." *Journal of Neural Engineering* 17: 046003. https://doi.org/10.1088/1741-2552/ab9b6d.

Field, M., V. Dorovykh, P. Thomas, and T. G. Smart. 2021. "Physiological Role for GABAA Receptor Desensitization in the Induction of Long-Term Potentiation at Inhibitory Synapses." *Nature Communications* 12: 2112. https://doi.org/10.1038/s41467-021-22420-9.

Froy, O. 2010. "Metabolism and Circadian Rhythms—Implications for Obesity." *Endocrine Reviews* 31: 1–24. https://doi.org/10.1210/er.2009-0014.

Gao, H., and B. N. Smith. 2010. "Tonic GABAA Receptor-Mediated Inhibition in the Rat Dorsal Motor Nucleus of the Vagus." *Journal of Neurophysiology* 103: 904–914. https://doi.org/10.1152/jn.00511.2009.

Germain, A., and D. J. Kupfer. 2008. "Circadian Rhythm Disturbances in Depression." *Human Psychopharmacology: Clinical and Experimental* 23: 571–585. https://doi.org/10.1002/hup.964.

Groves, D. A., and V. J. Brown. 2005. "Vagal Nerve Stimulation: A Review of Its Applications and Potential Mechanisms That Mediate Its Clinical Effects." *Neuroscience and Biobehavioral Reviews* 29: 493–500. https://doi.org/10.1016/j.neubiorev.2005.01.004.

Guo, Y. i.-F., and P. K. Stein. 2003. "Circadian Rhythm in the Cardiovascular System: Chronocardiology." *American Heart Journal* 145: 779–786. https://doi.org/10.1016/S0002-8703(02)94797-6.

Halliwill, J. R., and G. E. Billman. 1992. "Effect of General Anesthesia on Cardiac Vagal Tone." *American Journal of Physiology* 262: H1719–H1724. https://doi.org/10.1152/ajpheart.1992.262.6.H1719.

Hirota, K., A. Masuda, and Y. Ito. 1999. "Volatile Anesthetics Reduce Calcium Current in Parasympathetic Neurons From Bullfrog Hearts." *Anesthesia & Analgesia* 89: 225–229. https://doi.org/10.1097/00000539-199907000-00041.

Jenkins, A., E. P. Greenblatt, H. J. Faulkner, et al. 2001. "Evidence for a Common Binding Cavity for Three General Anesthetics Within the GABAA Receptor." *Journal of Neuroscience* 21: RC136. https://doi.org/10.1523/JNEUROSCI.21-06-j0002.2001.

Jiman, A. A., D. C. Ratze, E. J. Welle, et al. 2020. "Multi-Channel Intraneural Vagus Nerve Recordings With a Novel High-Density Carbon Fiber Microelectrode Array." *Scientific Reports* 10: 15501. https://doi.org/10.1038/s41598-020-72512-7.

Johnson, R. L., and C. G. Wilson. 2018. "A Review of Vagus Nerve Stimulation as a Therapeutic Intervention." *Journal of Inflammation Research* 11: 203–213. https://doi.org/10.2147/JIR.S163248.

Kameyama, K., K. Aono, and K. Kitamura. 1999. "Isoflurane Inhibits Neuronal Ca^{2+} Channels Through Enhancement of Current Inactivation." *British Journal of Anaesthesia* 82: 402–411. https://doi.org/10.1093/bja/82.3.402.

Kato, M., T. Komatsu, T. Kimura, F. Sugiyama, K. Nakashima, and Y. Shimada. 1992. "Spectral Analysis of Heart Rate Variability During Isoflurane Anesthesia." *Anesthesiology* 77: 669–674. https://doi.org/10.1097/00000542-199210000-00009.

Kotamraju, B. P., T. E. Eggers, G. A. McCallum, and D. M. Durand. 2023. "Selective Chronic Recording in Small Nerve Fascicles of Sciatic Nerve With Carbon Nanotube Yarns in Rats." *Journal of Neural Engineering* 20: 066041. https://doi.org/10.1088/1741-2552/ad1611.

Krizo, J. A., and E. M. Mintz. 2015. "Sex Differences in Behavioral Circadian Rhythms in Laboratory Rodents." *Frontiers in Endocrinology* 5: 234. https://doi.org/10.3389/fendo.2014.00234.

Lake, D. E., J. S. Richman, M. P. Griffin, and J. R. Moorman. 2002. "Sample Entropy Analysis of Neonatal Heart Rate Variability." *American Journal of Physiology. Regulatory, Integrative and Comparative Physiology* 283: R789–R797. https://doi.org/10.1152/ajpregu.00069.2002.

Leung, C. G., and P. Mason. 1995. "Effects of Isoflurane Concentration on the Activity of Pontomedullary Raphe and Medial Reticular Neurons in the Rat." *Brain Research* 699: 71–82. https://doi.org/10.1016/0006-8993(95)00858-N.

Li, X., M. L. Shaffer, S. Rodriguez-Colon, et al. 2011. "The Circadian Pattern of Cardiac Autonomic Modulation in a Middle-Aged Population." *Clinical Autonomic Research* 21: 143–150. https://doi.org/10.1007/s10286-010-0112-4.

Magnuson, M. E., G. J. Thompson, W.-J. Pan, and S. D. Keilholz. 2014. "Time-Dependent Effects of Isoflurane and Dexmedetomidine on Functional Connectivity, Spectral Characteristics, and Spatial Distribution of Spontaneous BOLD Fluctuations: TIME DEPENDENT BOLD PROPERTIES UNDER DEXMED FOLLOWING ISOFLURANE." *NMR in Biomedicine* 27: 291–303. https://doi.org/10.1002/nbm.3062.

Makino, M., H. Hayashi, H. Takezawa, M. Hirai, H. Saito, and S. Ebihara. 1997. "Circadian Rhythms of Cardiovascular Functions Are Modulated by the Baroreflex and the Autonomic Nervous System in the Rat." *Circulation* 96: 1667–1674. https://doi.org/10.1161/01.CIR.96.5.1667.

Marmerstein, J. T., G. A. McCallum, and D. M. Durand. 2021. "Direct Measurement of Vagal Tone in Rats Does Not Show Correlation to HRV." *Scientific Reports* 11: 1210. https://doi.org/10.1038/s41598-020-79808-8.

Marmerstein, J. T., G. A. McCallum, and D. M. Durand. 2022. "Decoding Vagus-Nerve Activity With Carbon Nanotube Sensors in Freely Moving Rodents." *Biosensors* 12: 114. https://doi.org/10.3390/bios12020114.

Marmerstein, J. T., G. McCallum, A. Rodrigues, and D. Durand. 2023. "Decoding Vagus Nerve Activity With Carbon Nanotube Sensors in Freely Moving Rodents." https://doi.org/10.26275/DO5J-MZ5Q.

McCallum, G. A., J. Shiralkar, D. Suciu, et al. 2020. "Chronic Neural Activity Recorded Within Breast Tumors." *Scientific Reports* 10: 14824. https://doi.org/10.1038/s41598-020-71670-y.

McCallum, G. A., X. Sui, C. Qiu, et al. 2017. "Chronic Interfacing With the Autonomic Nervous System Using Carbon Nanotube (CNT) Yarn Electrodes." *Scientific Reports* 7: 11723. https://doi.org/10.1038/s41598-017-10639-w.

Micera, S., P. M. Rossini, J. Rigosa, et al. 2011. "Decoding of Grasping Information From Neural Signals Recorded Using Peripheral Intrafascicular Interfaces." *Journal of Neuroengineering and Rehabilitation* 8: 53. https://doi.org/10.1186/1743-0003-8-53.

Miller, A. L., H. D. R. Golledge, and M. C. Leach. 2016. "The Influence of Isoflurane Anaesthesia on the Rat Grimace Scale." *PLoS One* 11: e0166652. https://doi.org/10.1371/journal.pone.0166652.

Morrison, J., and S. Pearson. 1989. "The Effect of the Circadian Rhythm of Vagal Activity on Bronchomotor Tone in Asthma." *British Journal of Clinical Pharmacology* 28: 545–549. https://doi.org/10.1111/j.1365-2125.1989.tb03540.x.

Nagaraj, N., and K. Balasubramanian. 2017. "Three Perspectives on Complexity: Entropy, Compression, Subsymmetry." *European Physical Journal Special Topics* 226: 3251–3272. https://doi.org/10.1140/epjst/e2016-60347-2.

Nemenman, I., W. Bialek, and R. de Ruyter van Steveninck. 2004. "Entropy and Information in Neural Spike Trains: Progress on the Sampling Problem." *Physical Review E* 69: 056111. https://doi.org/10.1103/PhysRevE.69.056111.

Ogawa, M., S. Zhou, A. Y. Tan, et al. 2007. "Left Stellate Ganglion and Vagal Nerve Activity and Cardiac Arrhythmias in Ambulatory Dogs With Pacing-Induced Congestive Heart Failure." *Journal of the American College of Cardiology* 50: 335–343. https://doi.org/10.1016/j.jacc.2007.03.045.

Oosting, J., H. A. J. Struijker-Boudier, and B. J. A. Janssen. 1997. "Autonomic Control of Ultradian and Circadian Rhythms of Blood Pressure, Heart Rate, and Baroreflex Sensitivity in Spontaneously Hypertensive Rats." *Journal of Hypertension* 15: 401–410. https://doi.org/10.1097/00004872-199715040-00011.

Ouyang, W., and H. C. Hemmings. 2005. "Depression by Isoflurane of the Action Potential and Underlying Voltage-Gated Ion Currents in Isolated Rat Neurohypophysial Nerve Terminals." *Journal of Pharmacology and Experimental Therapeutics* 312: 801–808. https://doi.org/10.1124/jpet.104.074609.

Paninski, L. 2003. "Estimation of Entropy and Mutual Information." *Neural Computation* 15: 1191–1253. https://doi.org/10.1162/089976603321780272.

Pardo, J. V., S. A. Sheikh, M. A. Kuskowski, et al. 2007. "Weight Loss During Chronic, Cervical Vagus Nerve Stimulation in Depressed Patients With Obesity: An Observation." *International Journal of Obesity* 31: 1756–1759. https://doi.org/10.1038/sj.ijo.0803666.

Picker, O., T. W. L. Scheeren, and J. O. Arndt. 2001. "Inhalation Anaesthetics Increase Heart Rate Bydecreasing Cardiac Vagal Activity Indogs." *British Journal of Anaesthesia* 87: 748–754. https://doi.org/10.1093/bja/87.5.748.

Picq, C. A., D. Clarençon, V. E. Sinniger, B. L. Bonaz, and J.-F. S. Mayol. 2013. "Impact of Anesthetics on Immune Functions in a Rat Model of Vagus Nerve Stimulation." *PLoS One* 8: e67086. https://doi.org/10.1371/journal.pone.0067086.

Qu, L., L. Dai, M. Stone, Z. Xia, and Z. L. Wang. 2008. "Carbon Nanotube Arrays With Strong Shear Binding-On and Easy Normal Lifting-Off." *Science* 322: 238–242. https://doi.org/10.1126/science.1159503.

Quigg, M. 2000. "Circadian Rhythms: Interactions With Seizures and Epilepsy." *Epilepsy Research* 42: 43–55. https://doi.org/10.1016/S0920-1211(00)00157-1.

Refinetti, R., G. Cornélissen, and F. Halberg. 2007. "Procedures for Numerical Analysis of Circadian Rhythms." *Biological Rhythm Research* 38: 275–325. https://doi.org/10.1080/09291010600903692.

Richman, J. S., and J. R. Moorman. 2000. "Physiological Time-Series Analysis Using Approximate Entropy and Sample Entropy." *American Journal of Physiology* 278: H2039–H2049. https://doi.org/10.1152/ajpheart.2000.278.6.H2039.

Rieke, F., D. Warland, R. R. van, de Ruyter Steveninck, and W. S. Bialek. 1999. "Spikes: Exploring the Neural Code." In *Computational Neuroscience* (First MIT Press paperback edition). MIT Press.

Silverman, H. A., A. Stiegler, T. Tsaava, et al. 2018. "Standardization of Methods to Record Vagus Nerve Activity in Mice." *Bioelectronic Medicine* 4: 3. https://doi.org/10.1186/s42234-018-0002-y.

Sinon, C. G., A. Ottensmeyer, A. N. Slone, et al. 2021. "Prehabilitative Exercise Hastens Recovery From Isoflurane in Diabetic and Non-Diabetic Rats." *Neuroscience Letters* 751: 135808. https://doi.org/10.1016/j.neulet.2021.135808.

Smets, H., L. Stumpp, J. Chavez, et al. 2022. "Chronic Recording of the Vagus Nerve to Analyze Modulations by the Light–Dark Cycle." *Journal of Neural Engineering* 19: 046008. https://doi.org/10.1088/1741-2552/ac7c8f.

Strong, S. P., R. Koberle, R. R. de Ruyter van Steveninck, and W. Bialek. 1998. "Entropy and Information in Neural Spike Trains." *Physical Review Letters* 80: 197–200. https://doi.org/10.1103/PhysRevLett.80.197.

Sugano, A., H. Murai, S. Horiguchi, et al. 2021. "Influence of Light–dark Cycle on Delayed Recovery from Isoflurane Anesthesia Induced by Hypnotics in Mice." *Journal of Pharmacological Sciences* 145, no. 4: 335–339. https://doi.org/10.1016/j.jphs.2021.02.003.

Tavakkolizadeh, A., A. Ramsanahie, L. L. Levitsky, et al. 2005. "Differential Role of Vagus Nerve in Maintaining Diurnal Gene Expression Rhythms in the Proximal Small Intestine1." *Journal of Surgical Research* 129: 73–78. https://doi.org/10.1016/j.jss.2005.05.023.

Victor, J. D. 2002. "Binless Strategies for Estimation of Information From Neural Data." *Physical Review E* 66: 051903. https://doi.org/10.1103/PhysRevE.66.051903.

Wagner, J. 2022. "The Vagus Nerve: Current Concepts in Anaesthesia and ICU Management." *South African Journal of Anaesthesia and Analgesia* 28: 193–197. https://doi.org/10.36303/SAJAA.2022.28.5.2811.

Wakai, A., T. Kohno, T. Yamakura, M. Okamoto, T. Ataka, and H. Baba. 2005. "Action of Isoflurane on the Substantia Gelatinosa Neurons of the Adult Rat Spinal Cord." *Anesthesiology* 102: 379–386. https://doi.org/10.1097/00000542-200502000-00021.

Wang, Q., R. Fong, P. Mason, A. P. Fox, and Z. Xie. 2014. "Caffeine Accelerates Recovery From General Anesthesia." *Journal of Neurophysiology* 111: 1331–1340. https://doi.org/10.1152/jn.00792.2013.

Wasilczuk, A. Z., C. Rinehart, A. Aggarwal, et al. 2024. "Hormonal Basis of Sex Differences in Anesthetic Sensitivity." *Proceedings of the National Academy of Sciences* 121, no. 3: e2312913120. https://doi.org/10.1073/pnas.2312913120.

Wodlinger, B., and D. M. Durand. 2009. "Localization and Recovery of Peripheral Neural Sources With Beamforming Algorithms." *IEEE Transactions on Neural Systems and Rehabilitation Engineering* 17: 461–468. https://doi.org/10.1109/TNSRE.2009.2034072.

Woodie, L. N., L. C. Melink, M. Midha, et al. 2024. "Hepatic Vagal Afferents Convey Clock-Dependent Signals to Regulate Circadian Food Intake." *Science* 386: 673–677. https://doi.org/10.1126/science.adn2786.

Wu, X.-S., J.-Y. Sun, A. S. Evers, M. Crowder, and L.-G. Wu. 2004. "Isoflurane Inhibits Transmitter Release and the Presynaptic Action Potential." *Anesthesiology* 100: 663–670. https://doi.org/10.1097/00000542-200403000-00029.

Yan, C., P. Li, M. Yang, et al. 2022. "Entropy Analysis of Heart Rate Variability in Different Sleep Stages." *Entropy Basel Switz* 24: 379. https://doi.org/10.3390/e24030379.

Zhang, Y., H. Li, X. Zhang, et al. 2022. "Estrogen Receptor-A in Medial Preoptic Area Contributes to Sex Difference of Mice in Response to Sevoflurane Anesthesia." *Neuroscience Bulletin* 38: 703–719. https://doi.org/10.1007/s12264-022-00825-w.

Supporting Information

Additional supporting information can be found online in the Supporting Information section.